Paper:
Attia, H., Johnson, D., Wright, C. & Hilal, N. (2018). Robust superhydrophobic electrospun membrane fabricated by combination of electrospinning and electrospraying techniques for air gap membrane distillation. *Desalination, 446*, 70-82.
http://dx.doi.org/10.1016/j.desal.2018.09.001

Robust superhydrophobic electrospun membrane fabricated by combination of electrospinning and electrospraying techniques for air gap membrane distillation

Hadi Attia [a] , Daniel J. Johnson [a], Chris J. Wright [b], Nidal Hilal [a] *

[a]Centre for Water Advanced Technologies and Environmental Research (CWATER), College of Engineering, Swansea University, Fabian Way, Swansea SA1 8EN, UK.

[b] Biomaterials, Biofouling and Biofilms Engineering Laboratory (B3EL), The Systems and Process Engineering Centre (SPEC), College of Engineering, Swansea University, Fabian Way, Swansea SA1 8EN, UK

* Corresponding author: n.hilal@swansea.ac.uk

Abstract:

Membrane pore wetting is the main problem hindering long term stability of permeate flux quality in membrane distillation (MD) applications. A superhydrophobic membrane with micro and nanostructured surface features can offer a unique solution to resolve this issue. Thus, a modified electrospun membrane was fabricated using a combination of electrospinning and electrospraying. The membrane surface hydrophobicity was enhanced by constructing a beaded structure from spraying a mixture of non-fluorinated alumina (Al_2O_3) nanoparticles (NPs) mixed with low concentration of PVDF polymer on an electrospun base membrane made from PVDF. The results revealed that a rough surface with a hierarchical structure can be constructed, which could not only enhance the membrane hydrophobicity, but also further enhance the permeate efficiency by improving parameters such as flux and rejection. Additionally, the membrane hydrophobicity could be further tuned by controlling the bead spinning volume. Our study shows that the modified membrane with 7.8μm beads layer thickness has boosted the liquid entry pressure (LEP) by 61% from 15.5 psi and the water contact angle to 154°. The performance of modified membranes with different spraying volume (1-5 ml) along with the neat electrospun and commercial membranes were examined in an air gap membrane distillation (AGMD) application for 5 hours using a 2.5 wt% of synthetic heavy metal solution as a wastewater model. Then, the optimized superhydrophobic membrane with 2 ml spinning volume (ES15-2) was further tested in comparison with the commercial membrane during long-term operations (30 h) using 3.5 wt% of mixed heavy metals. The flux was 18.67 LMH (L m^{-2} h^{-1}) for modified membrane (ES15-2) compare with 12.62 LMH for commercial PVDF membrane during 30 h of long-term operation with feed and coolant temperature at 60°C, 20°C, respectively. The present superhydrophobic membrane fabricated by a combined electrospinning/electrospray method shows high potential for MD applications.

Keywords:

Electrospinning, Electrospray, Heavy metal treatment, Air gap membrane distillation, Superhydrophobic, Bead structure, Alumina NPs, Self-cleaning membrane.

1. Introduction:

Membrane distillation (MD) is an emerging separation process which has been applied to different sectors, such as desalination of sea water, brackish water and removal of pollutants from wastewater. MD can play a significant role in treatment of wastewater polluted with heavy metals, which is a major environmental concern threatening public health worldwide. This is due to the unique advantages MD possesses, such as very high rejection of non-volatile compounds, moderate operation conditions such as temperature and pressure, lowered stress on membranes compared with pressure driven separation processes [1-3]. Nevertheless, MD experiences some obstacles to implementation in wastewater treatment, such as membrane durability (pore wetting) and relatively low permeate flux [3, 4].

MD is a thermal process (non-isothermal) where the permeate flux is achieved through a driving force created by a difference in a vapour pressure across a porous hydrophobic membrane [5]. Air gap membrane distillation (AGMD), which is one of four MD configurations: direct contact membrane distillation (DCMD), vacuum membrane distillation (VMD) and sweep gas membrane distillation (SGMD), has gained much attention. AGMD configuration functions by the transfer of vapour from the hot feed solution, which is in contact with the hydrophobic membrane surface, to the cold condenser surface via an air gap [5, 6]. AGMD offers a unique solution to mitigate the heat lost by conduction in DCMD applications by introducing an insulating air gap between the membrane and the cooling plate [5, 7]. However, AGMD suffers from low permeate flux compared with DCMD due to increase mass transfer resistance caused by the separating air gap [8].

To overcome these obstacles, extensive investigations are needed in the membrane fabrication sector to fabricate an adequate membrane. Recently, the electrospinning method, which uses high voltage to fabricate an electrospun membrane, has been increasingly investigated as a unique method for production of membranes with high hydrophobicity and permeate flux. This is due to controllable fibre size, which allows to enhance the membrane hydrophobicity and porosity compared with other fabrication techniques. However, membrane wettability, which is related to pore wetting, is still the greatest challenge to commercialization of MD [9]. This is due to the intrinsic properties of the polymer used in the fabrication process, such as polytetrafluoroethylene (PTFE), poly (vinylidene fluoride) (PVDF) which lacks superhydrophobic properties. Therefore, electrospun membranes fabricated from these polymers need further modification [3].

Generally, two techniques can be utilized to fabricate superhydrophobic membrane, either by increasing the membrane surface roughness of a low surface energy material or by lowering the surface energy of rough surface membrane [10, 11]. Many researchers have successfully increased electrospun membrane hydrophobicity by embedding the nanoparticles within the polymer dope solution to increase fibre roughness and lower the surface energy such as: PVDF-PTFE-CNT [12], PVDF-SiO_2 [13], PVDF-PTFE-TiO_2[14], PVDF-PTFE-GO [15], PVDF-Al_2O_3 [16], PVDF-Clay [17], PSF- Cera flava [18]. Among them, Al_2O_3 NPs possess excellent thermochemical properties, low toxicity and are cost-effective materials with easy chemical surface functionalization by covalent bonds due to abundant OH groups on the NPs surface [19]. Nevertheless, Al_2O_3 has relatively high thermal conductivity around 28 W/m K [19]. This might have slightly negative effect especially in the DCMD application due to increase the membrane thermal conductivity which lead to increase the heat loss by conduction.

Despite all the efforts to embed the NPs in the nanofibres structure, membrane wettability is still one of the main challenges which need to be addressed especially over long-term operation. Inspired by the Lotus effect, a superhydrophobic membrane with WCA above 150^{o}C and lower sliding angle can be fabricated to overcome pore wetting, in which a hieratical structure of the surface created by micro- and nano-structures can enhance surface hydrophobicity by introduction of air pockets between the rough surface and water drop. In general, different techniques can be used to achieve this goal, such as layer-by-layer [20, 21] , chemical vapor deposition [22], spray-deposition [3] and electrospray [23]. Among them, electrospray is a simple method due to less steps needed compared with other techniques. Moreover, it can be integrated successfully with the electrospinning method to fabricate membrane with one-step. The advantage of this integration technique is fabricating a superhydrophobic membrane to mitigate pore wetting. However, the biggest hurdles are the stability of the spraying material on the membrane surface and maintaining membrane flux. Few studies have been investigated applying spraying technique for MD application. For example, Zhang et al. [24] explored the effect of NPs concentration in the spraying mixture of SiO_2 NPs and polydimethylsiloxane (PDMS) on water contact angle (WCA) and liquid entry pressure (LEP) using the air brush technique on flat sheet PVDF membrane made by phase inversion. The results revealed that an increase of SiO_2 NPs concentration in the spray mixture from 0 to 1.5 wt% led to an increase in LEP by 19.5 %, WCA by 45.8% from 33.3 psi and 107^{o}, respectively. However, the permeate flux suffered a reduction of around 38 % from 13 LMH, when coating the neat membrane with 1.89 μm thickness, using DCMD application in which 70^{o}C and 20^{o}C was used as a feed and coolant temperature, respectively. In another study, Shaahbadi and his co-authors [23] investigated an electrospray mixture of TiO_2 NPs with poly vinylidene fluoride-co-hexafluoropropene (PH) polymer on a PH electrospun membrane. Their results revealed that the modified membrane used in DCMD with a top electrosprayed layer of 25 μm over 100μm of base membrane had a higher WCA around 162^{o} and water flux 38 LMH. However, the modified membrane had a low LEP (1.1 bar) which they explained was due to possess the membrane high pore size around 0.7 μm. Very recently, Makanjuola et al. [3] fabricated a superhydrophobic electrospun membrane with WCA of 155^{o} and LEP of 22 psi. The electrospun membrane was fabricated by integrating the hydrophobic microparticles (teflon oligomer) with the membrane structure made from poly (vinylidenefluoride-co-hexafluoropropylene) nanofibers through pumping the microparticles into the electrospinning chamber every 10 minutes. This resulted in highly attached microparticles with the nanofibres. However, low permeate flux was recorded about 7 LMH with membrane mean pore size 0.57 μm and membrane thickness 30μm for DCMD application using 60^{o}C and 25^{o}C as feed and coolant temperature, respectively.

In this work, a novel approach was implemented to fabricate a superhydrophobic membrane with beaded surface features through one step production by combining electrospinning and electrospray techniques. Spraying volume of nonfluorinated superhydrophobic Al_2O_3 nanoparticles, which was dispersed in a solvent mixture (DMF: Acetone) and low concentration of PVDF polymer, were investigated in term of membrane morphology and performance. Additionally, membrane morphology and performance were characterised using scanning electron microscopy (SEM); water contact angle (WCA); sliding angle (SA); liquid entry pressure (LEP); mean, minimum and maximum pore size; tensile test; and thermal properties. Moreover, membrane performance for long duration operations (30 h) compared with a commercial membrane was also accomplished.

2. Materials and methods:

2.1 Materials

Polyvinylidene fluoride pellets (Mw = 275,000 g/mol), alumina (Al_2O_3) NPs (Mw = 101.96, particle size = 13 nm), hexadecyl trimethyl ammonium bromide (HTAB), dimethylformamide (DMF), acetone, toluene, ethanol, isopropanol were obtained from Sigma-Aldrich, UK. Isostearyl acid was supplied by Nissan Chemical Industries. Cadmium nitrate tetrahydrate, zinc nitrate hexahydrate, lead (II) nitrate, copper nitrate trihydrate, and nickel nitrate hexahydrate were purchased from Fisher Scientific. PVDF commercial membrane under the trade name HVHP was supplied by Millipore. High quality DI water was supplied by a Milli-Q plus water purification system (Direct 8, Millipore, USA) to prepare synthetic wastewater. Additionally, all chemicals were used without further purification.

2.2 Dope solution preparation

The dope solution for fabricating the neat electrospun membrane and the support layer for modified electrospun membranes was prepared using 15 wt% of PVDF polymer. The procedure was achieved by dissolving a specific amount of PVDF pellets in a well-blended mixture of HTAB with DMF and acetone, as shown in Table 1, at a stirring speed of 200 rpm and heating temperature of 50^{o}C in an incubator shaker (Innova 44R, New Brunswick Scientific, USA) for 12 h. After cooling the dope solution to the room temperature, a vacuum drying oven (VC20, SalvisLab, Switzerland) was used at 200 mbar and room temperature for 30 minutes to remove the solution bubbles.

Dope solution for modified membrane fabricated through using electrospray technique combined with electrospinning was prepared as follows. First, modified membrane with beaded structure without NPs was achieved by dissolving 6wt% of PVDF in DMF and acetone mixture without any additives. Modified membranes with NPs embedded in beaded structure were prepared by dispersing the alumina NPs in DMF solvent with the aid of a sonication bath (Transsonic T700/H, Elma, Germany) for 60 minutes before adding the acetone and 6 wt% PVDF pellets. Next, both modified solutions (with and without NPs) followed the same procedure of electrospinning dope solution using incubated shaker and vacuum oven. Superhydrophobic Al_2O_3 NPs were prepared by using a non-fluorinated functional group (isostearyl acids) to functionalize nascent nanoparticles, as we previously described [25, 26]. Furthermore, the dope solution viscosity was measured by taking the average value of the viscosity reading of the torque range (10-90 %) using a Rheometer (DV3 TLV, Brookfield Engineering Laboratories, USA) at 25^{o}C with spindle SC4–18. Dope solution electrical conductivity and surface tension was measured using a conductivity meter (3540 pH/ conductivity meter, Jenway, UK) and pendant drop method by using a drop shape analyser (DSA25, Krüss, Germany) at 25^{o}C, respectively.

Table 1. Dope solution composition and properties for electrospinning and electrospray layer.

Polymer solution code	PVDF (g)	DMF (g)	Acetone (g)	HTAB (g)	Al_2O_3 NP (g)	Viscosity (cP)	Conductivity (µs/cm)	Surface tension (mN/m)
15 wt%	3.532	12	8	0.01	------	118.0±0.5	45.9 ±0.7	31.17 ±0.17
6 wt%	1.278	12	8	-----	------	10.7 ±0.6	2.53 ±0.1	28.61±0.14
6 wt%+30 wt% NPs	1.278	12	8	-----	0.383	13.4 ±0.4	2.54 ±0.1	30.57±0.11

2.3 Membrane fabrication

The electrospun membranes were fabricated using a lab-made electrospinning device as shown in Fig. 1 with further details can be found in Attia et al. [27]. For neat membrane and support layer of modified membrane, the polymer solution was electrospun on a rotating drum covered by aluminium foil using a row of four needles (18 G) with two different flow rates (0.2 ml/h for middle two needles and 0.35 ml/h for needles positioned at either end) and a spinneret to drum space of 150 mm. In terms of modified membranes with beaded surface structure, the PVDF dope solution was sprayed on the surface of the PVDF membrane using one needle (22 G) and flow rate of 0.5 ml/h which was located 150 mm from the rotating drum. Additionally, the electrospray layer thickness was adjusted by varying the electrospray dope solution volume from 1 to 5 ml. The neat and modified membranes were dried at 35ºC for 3 hours to remove the residual solvent. Then, membranes were heat-pressed by applying pressure of about 6.27 kPa at a temperature of 160 °C for 1 hour. Further, the membranes were named according to base dope solution concentration and beaded spray volume (see Table 2). For instance, ES15-1 for 15 wt% PVDF concentration used for the based membrane layer and 1 ml for the spray volume whereas C in ES15-C was used for a control beaded membrane without NPs embedded in 2 ml spraying volume.

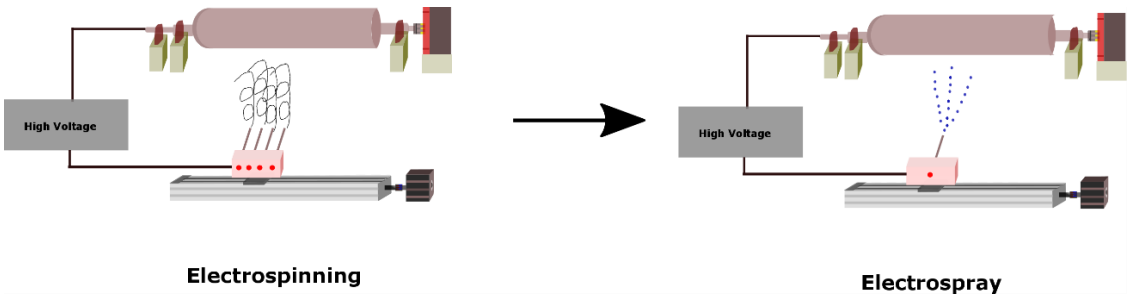

Fig. 1 The drum Electrospinning device used in this study for electrospinning and electrospray technique.

2.4 Membrane characterization

The morphology of the electrospun membranes (surface and cross-section) were characterized using a scanning electron microscope (S-4800, Hitachi, Japan) with acceleration voltage of 10 KV and current 5μA. In order to prepare the membrane for cross-section measurement tests, the membrane was submerged in liquid nitrogen first for 5 minutes following by snapping against the edge of a sharp scalpel blade. Membranes were coated with a conductive layer of chromium with a thickness 5 nm using a sputter coating system (Q150TS, Quorum Technologies, UK). The average diameter of nanofiber/microparticle was calculated from the measured of 100 nanofibers/microparticles diameter using ImageJ program in 3 randomly selected areas. Bead density was counted by taking the average of five different specific area measurements on the membrane surface with diameters measured by ImageJ program.

The mean, maximum and minimum pore size was determined by the bubble-point method. The custom-made setup consisted of a 50 ml stirred cell (8050 Amicon cell, Millipore Corporation, USA) having an effective area of 13.4 cm^2, which is described elsewhere [28].

The gravimetric method was used to calculate the electrospun membrane porosity. The test was accomplished by taking the weight of dry and wet membrane and using Eq. (1) to calculate the membrane porosity. The wet membrane measurements were achieved by submerging the dry membrane in isopropanol solvent for 10 minutes followed by removal the excess of the solvent by putting the membrane between two sheets of blotting paper.

$$\rho = \frac{(W_1 - W_2) \times de}{[(W_1 - W_2)/de] + \frac{W_2}{dp}} \quad (1)$$

Where ρ is the membrane porosity, W_1 is a saturated membrane with isopropanol weight in gram, W_2 is the dry membrane weight in gram, de is the isopropanol density in (g/m^3) and dp is the PVDF polymer density in (g/m^3).

Membrane thicknesses were evaluated using a digital micrometer (Series 293-IP65, Mitutoyo Corp, Japan) with a precision of ±1 μm, with quoted values being an average of 6 measurements. The thickness of the spray layer was measured using SEM.

Membrane wettability resistance and hydrophobicity was tested by using LEP, WCA and sliding angle. In terms of LEP, the test was conducted by using dead end filtration set-up where described extensively by Attia at el [28]. In brief, the electrospun and commercial membrane was accommodated in a low pressured cell (8050 Amicon cell, Millipore Corporation, USA) in which the pressure was supplied over deionized water (DI) and control by analogue pressure gauge through a nitrogen cylinder. During the measurement, nitrogen pressure was increased slowly in 1 psi steps by using a needle valve and maintained for 10 minutes. The pressure at which the DI water penetrates through the membrane is considered as the LEP. The sessile drop method was used to measure the water contact angle (WCA) with the help of the drop shape analyser (DSA25, Krüss, Germany). This test was carried out by fixing the electrospun membrane on a glass slide by double-sided adhesive tape before dropping 4 μL of DI water at different membrane surface locations. All values reported are an average of 5 individual measurements. Further, the slide angle (SA) was recorded by tilting the glass slide on which the membrane was fixed and recording the angle value when the 4 μL DI drop rolled off the membrane surface.

Mechanical properties for electrospun membranes were recorded using a universal testing machine (H25 KS, Hounsfield, UK) with a 100N loading cell, 40 mm gauge length, and 50 mm/min of crosshead speed according to ASTM D-638. A cardboard frame with the outside dimension (60 ×60 mm) and inside dimension (40×40 mm) was used to hold the delicate electrospun membrane with the help of double side adhesive tape, which was previously reported [29]. After securing the membrane in the device's jaws, cardboard frames were cut from the middle at the two sides by scissors before starting the test.

Membrane thermal property measurements for neat, modified and commercial membrane were carried out using differential scanning calorimetry (DSC) with a thermal analyser (SDT Q600, TA instruments, USA). In brief, around 6 grams of the cut membrane was placed in an alumina crucible followed by heating program from 50 to 250°C using heating rate of 10 °C/min and air flow rate 100 ml/min. This was followed by a cooling cycle from 250°C to ambient temperature after it had been kept under isothermal conditions for 5 minutes. Membrane melting temperature (Tm) which represents the peak of the melting endotherm during the heating cycle, the crystallization temperature (Tc) which represents the peak of crystallization exotherm during the cooling cycle, the enthalpy of melting (ΔH_m), and the heat of crystallization (ΔH_c) were measured using TA Universal analysis 2000 software (Version 4.5A Build 4.5.0.5), whereas the degree of crystallinity derived from the melting (X_m) or crystallization (X_c) were calculated from experimental data using Eq. (2) and (3) [30].

$$X_m = \frac{\Delta H_m}{\Delta H^o} \times 100 \quad (2)$$

$$X_c = \frac{\Delta H_c}{\Delta H^o} \times 100 \quad (3)$$

Where ΔH^o is the heat fusion of 100% crystalline PVDF which is equal to 104.6 kJ/kg [31].

2.5 AGMD performance test

Air gap membrane distillation (AGMD) was carried out to assess the permeate flux and rejection percentage for neat, modified electrospun membranes and commercial membrane. A schematic diagram of the lab-made AGMD apparatus is explained elsewhere [28]. In brief, a flat sheet membrane with an effective surface area of 28.26 cm^2 was placed on a horizontal stainless-steel membrane cell. A synthetic mixed solution of five heavy metal elements (Pb, Cd, Zn, Cu, Ni) with 500 and 600 ppm concentrations for each element were used as a feed solution for short and long-term operation, respectively. The electrical conductivity (EC) and pH of the 2500 ppm solution was 6.32 ms/cm and 5, while for the 3500 ppm solution the values were 7.55 ms/cm and 4.6 for EC and pH, respectively. Additionally, the synthetic wastewater quantities are shown in Table S1 by adding different heavy metals salts to DI water. The feed solution was maintained at 60°C by using a heater with control set-up in isolated take with feed volume of 10 litres. The feed flow rate was preserved at 1.5 l/min using a gear pump and it was monitored by using a glass flowmeter. The cooling side, with opposite flow direction to the feed solution and a flow rate of 8.5 l/min, was cooled by using a chiller and maintained at 7°C and 20°C for five and thirty hours as an operation time, respectively. The feed and cooling stream temperatures were recorded by using four T-type thermocouples. The permeate weight values were recorded every five minutes by the aid of Education Program (version 3.02, Precisa Instruments, Switzerland). The heavy metal concentration was measured by atomic adsorption spectroscopy (PinAAcl 900F, PerkinElmer, USA). Additionally, the permeate flux and rejection measured were measured as described in our previous publication [27].

3. Results and discussion

3.1 Surface morphology

Membrane surface morphology, including membrane roughness and topography, is considered one of the important parameter in accessing the membrane performance. Therefore, SEM images with the corresponding cross section and histograms of bead diameter distribution for modified membrane and fibres diameter distribution for nascent membrane were recorded. Fig 2 and Fig. 3 show the surface structure of commercial, unmodified and modified electrospun membranes (four different spinning volumes) fabricated by using a combination of electrospinning and electrospray techniques, whilst Table 1 and Table 2 illustrate the solution parameters and membrane properties, respectively. It can be seen from Fig. 2b that the neat electrospun membrane (ES15) had uniform, continuous and bead-free nanofibres as well as a porous structure with an average fibre diameter 236 nm. This electrospun membrane structure with bead-free nanofibre might be due to a moderate viscosity of the fabrication solution (118 cP) as a result of using 15 wt% as a polymer concentration. Additionally, using the cationic surfactant (HTAB) would reduce the surface tension of the dope solution and enhance dope solution conductivity [16, 27].

In order to create a hierarchical structure on the membrane surface for boosting membrane hydrophobicity, electrospray combined with electrospinning was used. The modified membrane surface was fabricated through creating a beaded structure on top of the unmodified and beadless electrospun membrane as base layer were investigated using four different spinning volumes. Firstly, the fabricating of modified membrane with beaded structure in the absence of Al_2O_3 NPs were achieved by spraying 6wt% PVDF. The reduction of the polymer concentration to 6 wt% without adding any additives created a beaded structure instead of nanofibre as shown in Fig. 2c. This might be due to lower entanglement of the polymer chain due to use low polymer concentration as reported by Lee et al. [32]. Additionally, the repulsion force between the polymer molecules, which has a positive charge, combined with the high surface tension of the polymer solution lead to creation of a beaded structure instead of more uniform fibre morphology. However, it can also be seen from Fig. 2c that some of the membrane area is covered with flattened beads, which might due to low polymer viscosity which is directly proportional with polymer concentration. Similar phenomenon has also been reported by Bock et al. [33] which emphases that the polymer concentration is the most critical parameter in the morphology of electrospray beads.

Adding Al_2O_3 NPs to the dope solution (6wt%) lead to production of nanostructures on the microbead surface, as shown in Fig. 4b, compared with smooth bead surfaces, shown in Fig. 4a. Adding Alumina NPs to the polymer dope solution lead to an increase the dope solution viscosity. For instance, adding 30wt% led to an increase in the viscosity by 25.2 % from 10.7 cP, which might help to reduce the number of flattened beads as well as produce smaller microbeads. Additionally, bead mean diameter reduced from 1.8 to 1.40 μm for ES15-C and ES15-2, respectively, which might be also due to the increase in dope solution viscosity. Details of bead diameter distributions for 10, 20 and 30 wt% of Alumina NPs with dope solution properties is shown in Fig. S1 and Table S2, respectively. Liu et al. [34] demonstrated that increased polymer viscosity leads to reduced bead size and number. It can also be seen from Fig. 2, 3 and 4 that every microbead is interlinked with each other by randomly interwoven nanofibers, with diameters in the range of 40-70 nm, which lead to increase the connection between the bead and the electrospun membrane. Shahabadi et al. [23] explained that polymer solutions with low concentration which have fewer polymer chain entanglements and weak viscoelastic forces can suffer from weak resistance to the electrostatic stretching force and this can lead to thinner fibre and bead structure.

Beads density and diameter distribution with 30 wt% embedded Al_2O_3 NPs was studied by varying the spraying volume from 1 to 5 ml. Fig. 2 and 3 shows that there is a broad beads diameter distribution with mean bead diameter around 1.33 μm. In terms of bead distribution, Fig. 3a-c shows uniform allocation of the deposited microbeads on the electrospun nanofibre surface especially with the spinning volume less than 3 ml. It can be seen that the bead density increased from 3.75 to 9.75 beads/μm and top layer thickness from 4.3 to 13.2 μm by increasing the spinning volume from 1 to 3 ml. While the whole membrane (ES15-5) in Fig. 3d was covered with randomly distributed bead in a multilayer structure and with a top layer thickness about 24μm, by using 5 ml as a spinning volume. In contrast, bead with a monodispersed layer was observed when using a spraying volume of 3 ml and less. The random distribution of beads when using 5 ml as a spinning volume might be due to the high repulsion between the beads, which leads to formation large micro-gaps on the membrane surface. Similar behaviour has previously been reported by Wu et al. [35] when spraying 10 wt% of PVDF solution which they attributed to the affinity of small beads towards larger beads.

Table *2.* Summary of the spinning and spraying volume with the layers thickness of neat and modified electrospun and beads dimeter and density for modified membranes.

Polymer solution code	*Spinning volume (ml)*		*Membrane thickness (μm)*		*Bead density (beads / μm²)*	*Average Bead diameter (μm)*
	Top	*Bottom*	*Top*	*Total*		
ES15	----	*16*	-----	*118±3.72*	------	-----
ES15-C	*2*	*16*	*5.4±0.59*	*113±3.23*	*5.37±0.24*	*1.80*
ES15-1	*1*	*16*	*4.3±0.63*	*117±1.33*	*3.75±0.5*	*1.28*
ES15-2	*2*	*16*	*7.8±0.35*	*115±0.82*	*5.75±0.92*	*1.40*
ES15-3	*3*	*16*	*13.2±1.2*	*120±0.50*	*9.75±0.65*	*1.39*
ES15-5	*5*	*16*	*23.9±2.8*	*125±0.96*	*All surface cover with beads*	*1.25*

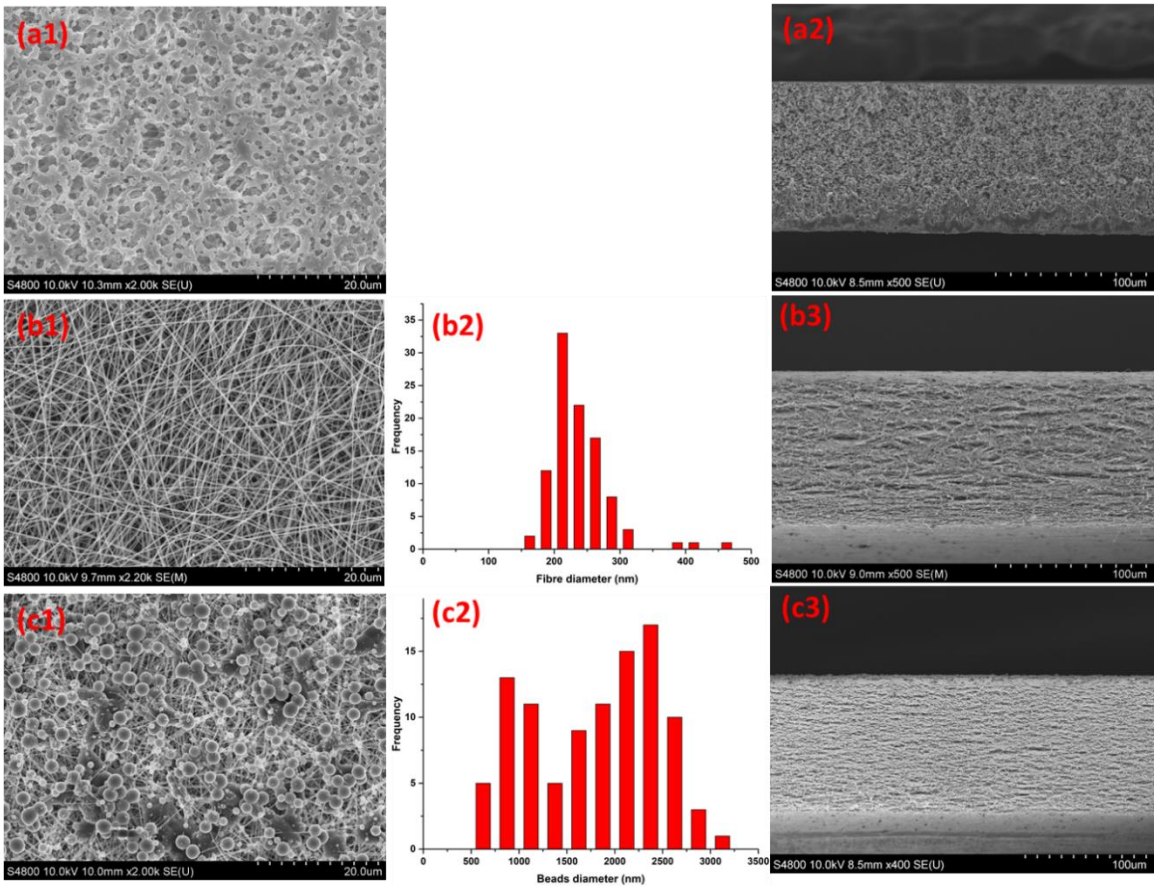

Fig. 2 SEM images, fibre diameter and beads distribution (a) commercial membrane HVHP, (b) neat membrane ES15, (c) modified membrane ES15-C.

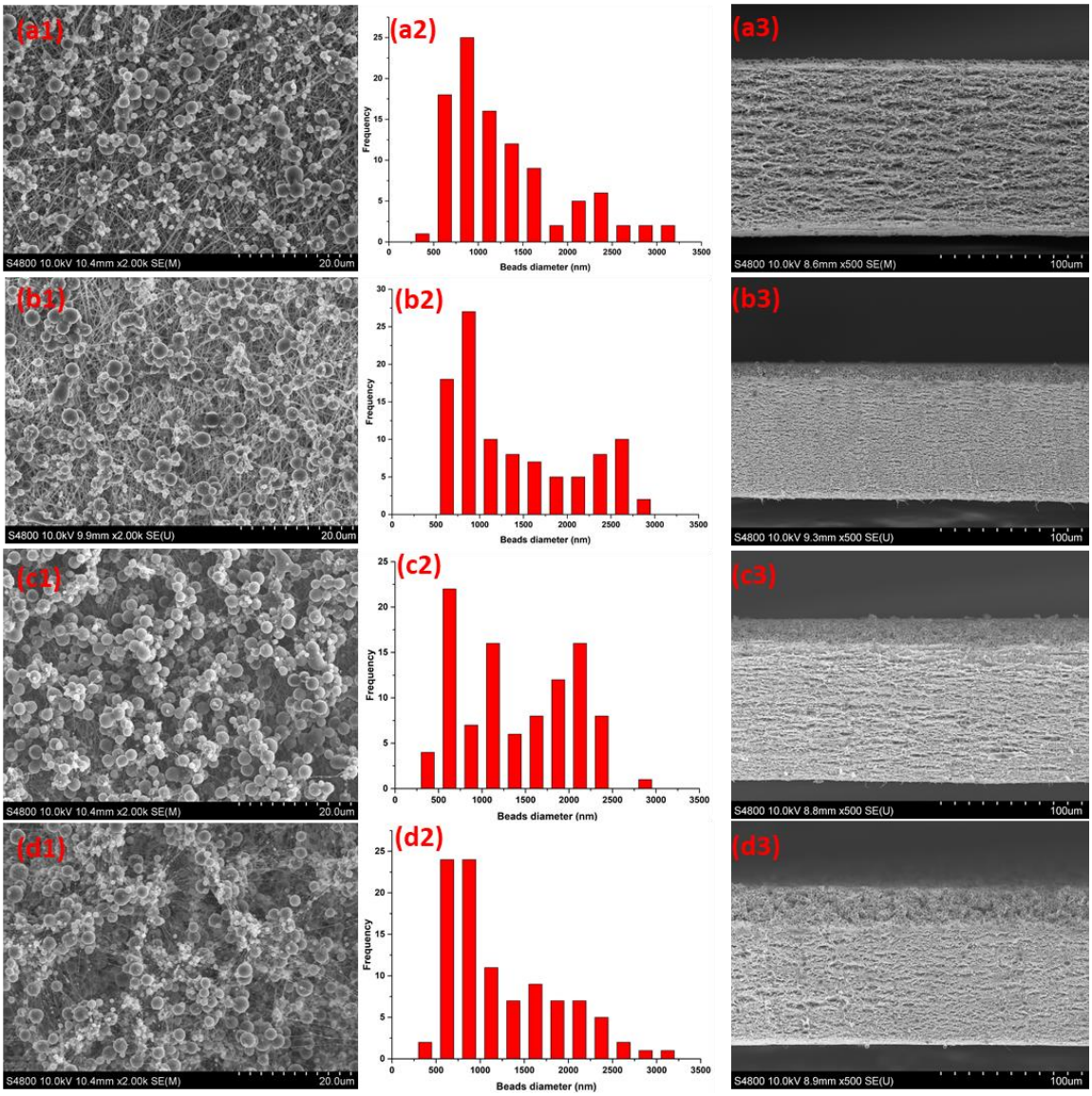

Fig. 3 SEM images of top surface, beads diameter and cross-section of modified electrospun membranes (a) ES15-1, (b) ES15-2, (c) ES15-3, (d) ES15-5.

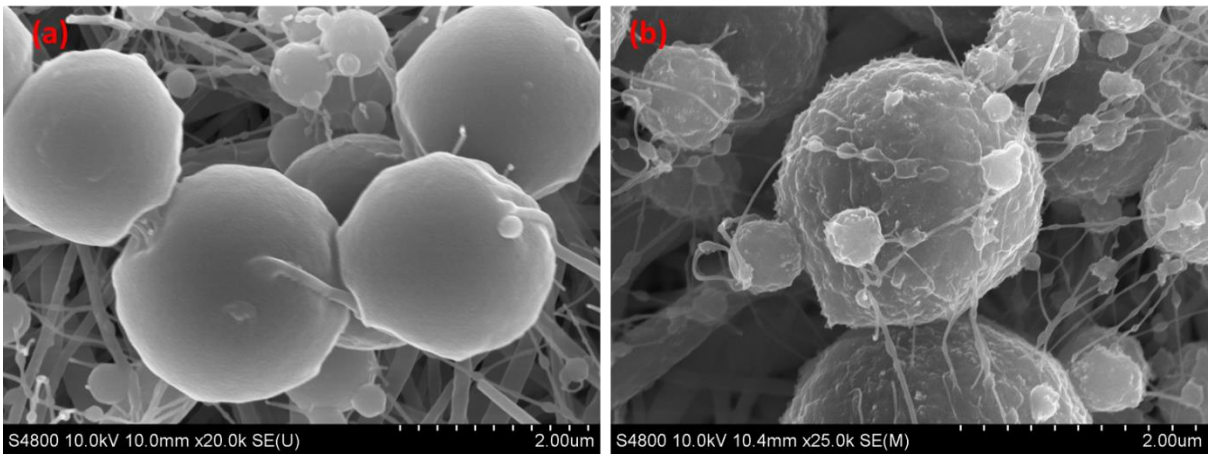

Fig. 4 SEM images of (a) beads without Alumina NPs (ES15-C), (b) Beads with 30% wt. Alumina NPs (ES15-2).

3.2 Membrane Surface wettability

Membrane wettability, or hydrophobicity, representing the interactions between the liquid and membrane surface is a crucial parameter for MD applications. In general, MD applications must use a membrane that is hydrophobic and has excellent water repellent properties to reduce membrane wettability, especially during long-time operations. This can be achieved by both reducing the membrane surface energy and increasing membrane roughness [36, 37]. In this section, unmodified and modified electrospun and commercial membranes were evaluated by using water contact angle (WCA) as well as the sliding angle (SA), shown in Fig. 5a. The water contact angle for neat electrospun membrane was 141^{o}, which is much higher than for the commercial membrane (HVHP) with a WCA value of 128°, where the membrane was fabricated by the phase inversion method. This can be attributed to high roughness of the electrospun membrane surface created by overlapping nanofibres, which leads to a reduction in the contact area between the water droplet and the membrane. This finding is similar with previously reported research work [23, 27].

Membrane modification with beaded structure was adopted to enhance membrane hydrophobicity and to improve the intrinsic properties of membrane roughness and surface energy. PVDF microbeads with and without coverage of superhydrophobic (non-fluorinated) alumina NPs was used to enhance membrane surface hydrophobicity. It can be seen from Fig. 5a that ES15-C membrane, which was fabricated by spraying 2 ml of microbeads structure on the neat electrospun membrane without adding NPs, enhanced the water contact angle from 141 to 148^{o}. This increase for WCA due to increase of membrane roughness by creating microstructure beads from PVDF polymer on the electrospun membrane surface. However, spraying of the bead structure on the membrane surface was insufficient to provide a superhydrophobic surface. This can be attributed to the lack of nanostructure on the beads surface to provide the hierarchical structure which would help to reduce the solid-water contact area and increase the amount of trap air on the beads surface besides beads voids. Moreover, the surface energy of the beads made from PVDF alone was not enough to provide the superhydrophobic state. Similar results were previously reported by Bahgat et al. [38].

Electrospun membranes modified with alumina NPs embedded in the bead structures showed a better outcome. Firstly, increased the NPs concentration was investigated on membrane hydrophobicity by varying from 10 to 30% using 2ml as a spring layer. The result showed that increase the Al_2O_3 NPs from 10 to 30 wt% led to increase the WCA from 150^{o} to

154^{o}. Therefore, 30 wt% for alumina NPs was considered as optimum additives for further investigation.

In terms of studying the effect of spraying dope solution volume, the result showed that increasing the spraying volume from 1 to 2 ml led to increase the water contact angle from 147^{o} to 154°. This can be attributed to both increasing of the membrane roughness (micro roughness) by increasing the bead density on the membrane surface and increasing the nano roughness by adding Al_2O_3 NPs. Liao et al. [39] demonstrated that an increase of spraying layer thickness leads to an enhancement of the hierarchical structure of the membrane surface. The water contact angle of this kind of rough surface would be expected to be described by the Cassie-Baxter wetting state, which describes heterogenous surfaces [40]. Increasing the air trapped underneath the water droplet, due to the bead surface structure in our case, leads to an increase of the liquid-vapour interfacial area and therefore increase membrane hydrophobicity.

Furthermore, compared with ES15-2, the hydrophobicity of E15-5 was decreased despite the high density of beads which might be due to created larger micro groove structures between the bead structures as shown in Fig 3d. This can be attributed to the transition from a Cassie-Baxter to a Cassie impregnating wetting state. Feng et al. [41] pointed out that the surface can be transited from Cassie-Baxter to Cassie impregnating states due to the difference in micro- and nano-structure by increasing the size of micro grooves in the surface nanostructure. Additionally, they mentioned that in the Cassie impregnating state water droplets would be expected to wet the large grooves while leaving the small grooves dry.

To assess adhesion forces between the water molecules and the membrane surface, sliding angle measurements were implemented for unmodified, modified and commercial membranes. Unmodified and commercial membranes showed high adhesion with the water drop in which water droplet could not roll off from the membranes surface even with turning the membranes upside down (i.e. SA > 90°). As a result, no value for SA is recorded in Figure 5a. In terms of electrospun membrane, this can be attributed to both large-scale grooves created between the nanofibres and surface tension force which lead to penetration of water droplets. A similar result was achieved by Lia et al. [39] which they refer to this phenomena as the petal effect.

On the other hand, modified membrane with bead structures formed by electrospraying onto nanofibre membrane surface with and without NPs showed contrary results. In terms of beaded membrane without NPs (ES15-C) the sliding angle cannot be measured due to the tendency of the water droplets to adhere to the membrane surface even when turning the membrane upside down. Beads with NP structures illustrated different result. First, membranes with nanofibres and bead structure on the top surface (ES15-2, ES15-3 and ES15-5) showed an increase of sliding angle with change from mono to multilayer beads structure. This can be attributed to a decrease of air pocket area (with water contact angle 180^{o}) between the beads by increased bead density, especially with the case of ES15-5 which illustrates a slightly higher SA of around 80^{o}.

3.3 Membrane pore size and Liquid entry pressure

Membrane internal structure which, was created by random accumulated of nanofibres as well as surface modification, can affect both pore size and liquid entry pressure. Generally, membrane pore size must be sufficiently high to allow high vapour flux, but at the same time must be small enough to maintain a high LEP [42]. In terms of membrane pore size, Fig. 5c shows the membrane mean, maximum and minimum pore size for neat and modified membranes and commercial membrane. It can be seen from Fig. 5c that the mean pore size of neat (i.e. electrospun base layer) membrane was 0.507 µm whereas minimum and maximum

pore size was 0.488 and 0.64, respectively. The membrane pore size for membranes fabricated by electrospinning is controlled by the fibre diameter [16, 27]. In addition, polymer viscosity, which corresponds with the polymer concentration and the polymer molecular weight, has a major effect on fibre diameter [43]. A moderate polymer viscosity of 118 cP led to produce a fibre diameter of 236 nm. Additionally, the mean pore size is slightly higher than our previous results [16] with mean pore size was 0.47µm due to using a multi-needle setup for electrospinning device. Commercial membrane (HVHP), on the other hand, which has a sponge-like structure as shown in Fig. 2a, showed a mean pore size 0.46 µm, which is closed to the manufacturers data.

In terms of modified membrane, the mean pore size was reduced slightly with the increase of spinning volume to 2 ml for ES15-C. This can be attributed to beaded structure of modified membrane which might altered the pore entrance. On the other hand, modified membrane with NPs embedded inside beaded structure show further reduction of membrane pore size with the increase of spinning volume. This can be due to an increase of bead density on the membrane surface with the increase of spinning volume, as shown in Fig. 3 and reduction in beads size as shown before. Moreover, embedded NPs with the beaded structure showed a variety in beaded shape which might played a significant role to alter the pore entrance. However, increase the spinning volume above 2 ml showed slightly increase in the membrane pore size. This might be attributed to strong repulsion between the beads on the membrane surface which carried high charge specially with multi-layers beads build-up as we can be seen from Fig. 3 on the membrane surface which lead to less compact structure during the heat-press procedure, which is in accordance with the results reported by Shahabadi et al. [23].

Beside membrane pore size, LEP can be controlled by different parameters. According to the Young-Laplace equation [9], LEP is governed by membrane pore geometry, maximum pore size, membrane hydrophobicity which represented by liquid contact angle on the membrane surface and liquid solution surface tension [9, 32, 44]. It can be seen from Fig. 5b that the commercial membrane showed the lowest LEP (14.5 psi), followed by neat membrane (ES15) with LEP 15.5 psi. This difference, according to the Young-Laplace equation, can be attributed mainly to membrane hydrophobicity created by different fabrication methods in which the WCA were 128 and 141^{o} for HVHP and ES15, respectively. Additionally, despite the slightly larger mean and maximum pore size for ES15 compared with HVHP in which mean and maximum pore size were 0.507, 0.64 and 0.46, 0.59 µm for ES15 and HVHP, respectively.

Modified membranes, on the other side, showed significant increases in LEP values. Firstly, electrospun membrane (ES15-C) with beaded surface structure (2 ml spinning without NPs) boosted the LEP by 22.6% compare with neat electrospun membrane (ES15). In comparison, ES15-2 illustrated the highest LEP at 25 psi. This sharp increase in LEP is mainly due to increase the membrane surface hydrophobicity according to the Young-Laplace equation in which the WCA for ES15-2 is 154^{o} while it is 148^{o} for ES15-C while there was 22 % reduction in membrane maximum pore size for ES15-2. Similar results were found by Liao et al. [39] who reported LEP values around 25 psi by using a beaded structure fabricated from 5 wt% PVDF mixed with fluorinated SiO_2 NPs with mixing ratio 1:2 as a top layer. Increase of the spinning volume beyond 2 ml has a slightly negative effect on LEP value. For example, E15-3 and E15-5 showed a reduction in LEP value to 24.5 and 21.6 respectively. This might be due to a reduction in WCA and change in the membrane surface morphology by creating larger micro grooves when increasing the spinning volume above 2 ml. Furthermore, it has previously been demonstrated that altering the wetting of the membrane surface by increase groove volume leads to a decrease in the LEP by reduction of the WCA [41].

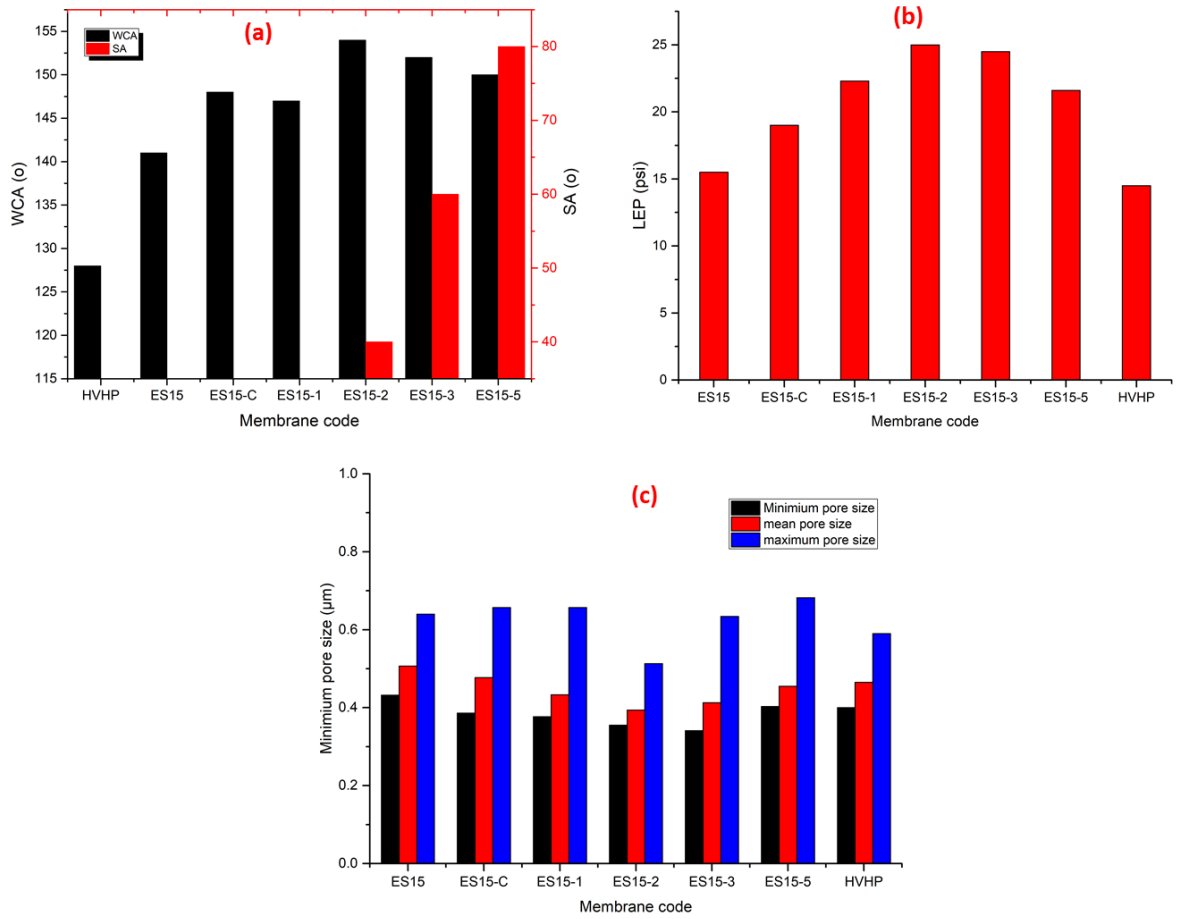

Fig. 5 (a) Membrane water contact angle and slide angle, (b) membrane liquid entry pressure, (c) membrane pore size.

3.4 Membrane porosity

Membrane porosity which is another important parameter for MD applications, which mainly affects the permeate flux. Therefore, the trade-off between the membrane porosity and hydrophobicity must be considered. In general, a membrane with high porosity minimizes the mass transfer resistance through greater surface area enhancing vapour transport , as well as reduction in heat loss due to more void space [42]. Fig. 6 shows the porosity of electrospun and commercial membranes. The electrospun membrane showed a 38.6 % increase in the porosity compared with the commercial membrane (HVHP) due to the structure created by overlapping fibres using electrospinning technique. Similar results for ES15 were reported previously [16]. However, modified membrane with micro-spherical bead coating illustrated a reduced membrane porosity compared with unmodified electrospun membrane, especially with high coating thickness, but porosity was still greater than that of the commercial membrane. Increasing the spinning volume of the bead layer led to a decrease in the membrane porosity (Fig. 6). This can be attributed to both membrane compression and the bead structures. The heat treatment of the electrospun membrane will reduce the prominence of the micro-spherical beads, further compressing the membrane. Additionally, the bead layer thickness, which was increased by increased the spinning volume leads to further reduction of the voids in the membrane structure, for instance, the porosity of ES15-2 reduced by 2.89%, whereas ES15-5 decreased by 11.47% compare with ES15 membrane. Similar results were reported by Lee et

al. [32] in which the porosity dropped from 89.5 to 72.4 % by modifying the electrospun membrane surface with a bead structure made from poly(dimethylsiloxane) and PVDF polymer. In contrast, Shahabadi et al. [23] illustrated that the porosity of the modified membrane with 25μm thickness of beaded layer showed an insignificant change, with porosity percentage between 86 to 90%.

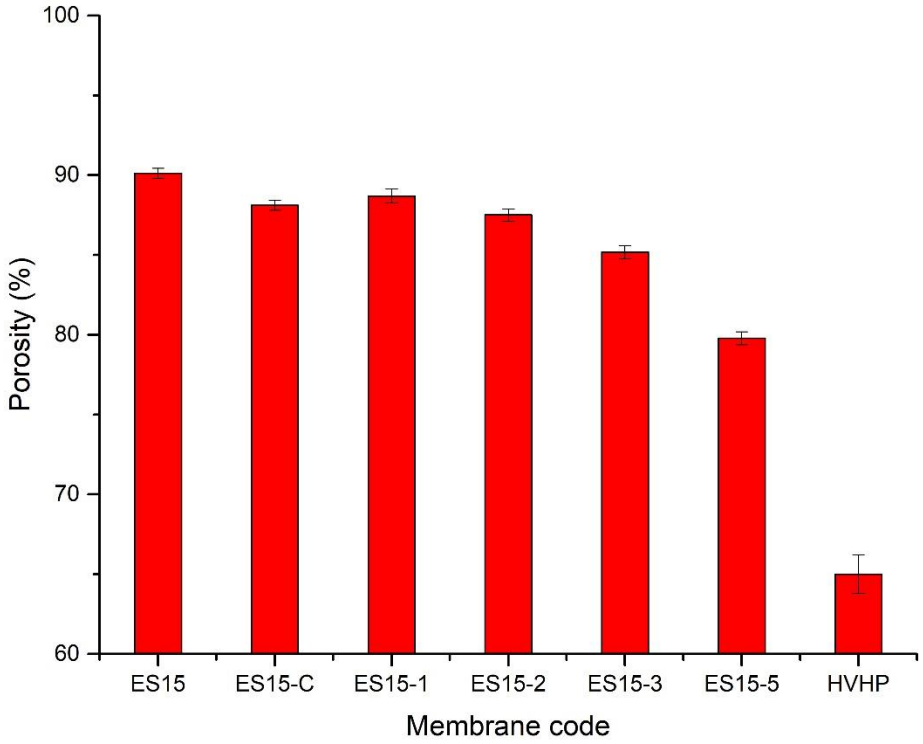

Fig. 6 membrane porosity for commercial, neat and modified membrane.

3.5 Membrane mechanical and thermal properties

Membrane mechanical and thermal properties affect membrane handling and performance when used in MD applications. Generally, MD operates under atmospheric pressure, therefore membrane mechanical requirement is less essential than for pressure derive membrane processes. However, due to membrane packing requirements as well as hydraulic impact, adequate mechanical properties are still needed to prevent membrane rapture. Hence, the mechanical properties of neat and modified electrospun membrane together with commercial membrane were investigated. Tensile-strain curves and the summary of the mechanical properties of the membranes are depicted in Fig. 7c and Table S3. It can be clearly seen that two different trends for stress-strain curve for electrospun and commercial membranes were observed. Electrospun membranes illustrated a nonlinear elastic deformation during the initial mechanical loading, followed by a linear increase until membrane breakage. However, commercial membrane had a sharp increase during the first 6% elongation and then gradually increased until rupture, which increased the Young's modulus by 71.6% compared with ES15. This is presumably due to the different fabrication methods used which created different membrane morphology. As can be seen in Fig. 2a, the commercial membrane illustrates a sponge-like structure with dense areas, while electrospun membrane shows a nonwoven structure with multidirectional fibres. Tijing et al. [42] point out that electrospun membrane might stretch in two different ways, depending upon how closely the fibres align with the

stretching direction. Fibres aligned with the pulling direction will be stretched uniaxially, while the fibres in other directions will undergo rotation to align themselves to the pulling direction.

It can be seen from the Fig. 7c that the neat membrane has high tensile strength and strain values compared with the commercial membrane. Table S3 shows that the tensile strength and strain for commercial membrane was 8.33 MPa and 37.86%, whereas for membrane ES15 it was 11.2 MPa and 86.71%, respectively.

Mechanical properties of modified membranes with bead structure were evaluated. It is well documented that the bead structure weakens the electrospun mat [45]. Hence, the bead microparticles effect on membrane tensile and strain was investigated. The results indicate that with the increase of spraying layer thickness, tensile strength reduces slightly whereas the elongation at break reduce significantly. For instance, the ES15-5 tensile strength and strain reduced by 40.5% and 66.5%, respectively compare with the neat membrane (ES15), whereas Young's modulus reduced by 28.6%. This difference in membrane stretching before rupture for the modified electrospun membrane could be explained by the effect of solvent evaporation from the bead structure during the electrospinning process and heat-press leading to further connection between the fibres which might hinder the nanofibers alignment in the applied load direction, causing the resulting beaded membrane to have lower stretching. Similar findings of reduction of tensile and strain values by modifying the electrospun membrane with a beaded structure using SiO_2 and PVDF has been reported by Liao group [39].

The thermal properties of the membranes, fabricated, from PVDF which has a semi-crystalline structure, were examined using DSC analysis to evaluate the effect of beads structure on membrane thermal stability. Fig. 7a and b show the relation between the temperature and heat flow for commercial, neat and modified membranes. It can be seen from Fig. 7a that the neat and modified membranes have a similar endothermic melting peak at around 168^{o}C, which is lower than the commercial membrane of 179°C. The results indicate that the bead structure of the modified the electrospun membrane has an insignificant effect on the membrane thermal properties. The degree of crystallinity of membranes are listed in Table S4. It can be seen that there is an insignificant change in the degree of crystallinity of the modified membrane.

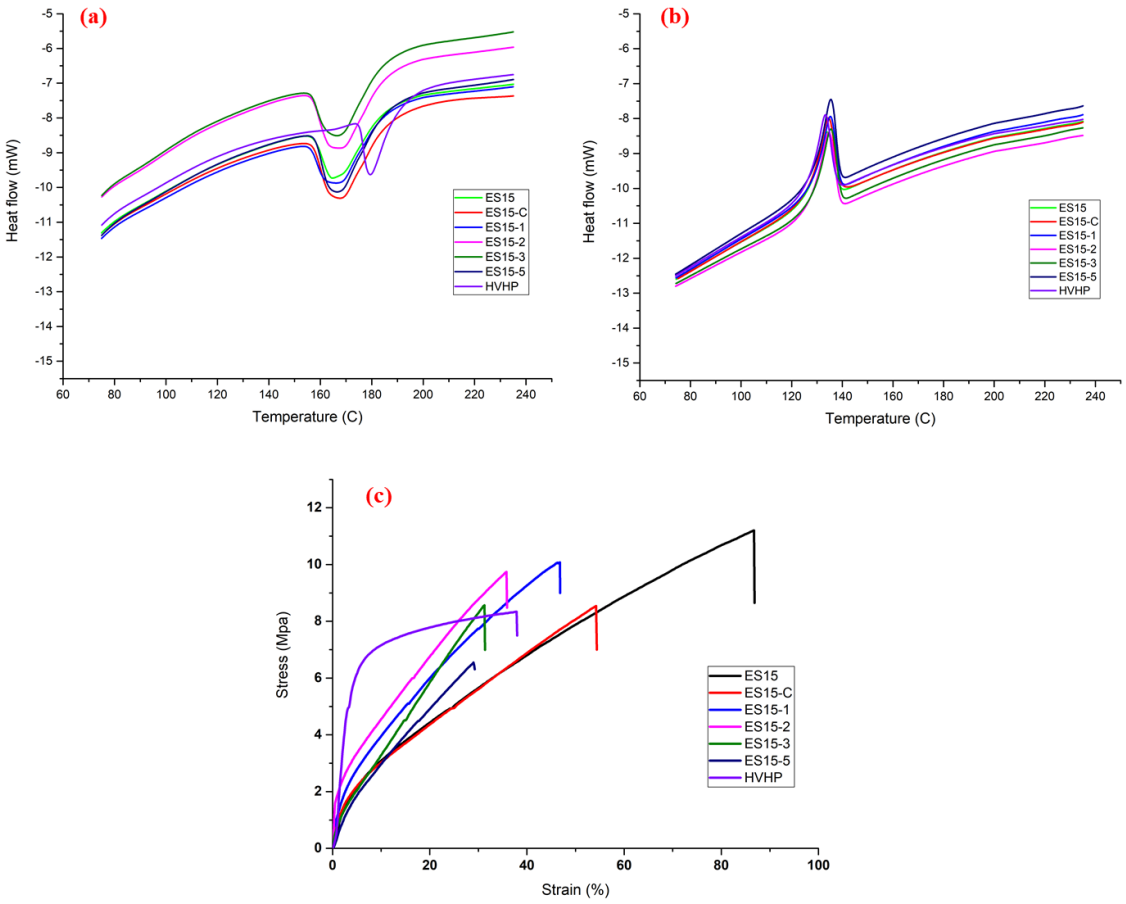

Fig. 7 Thermal and mechanical test for commercial and electrospun membrane (a) DSC test for heating cycle, (b) DSC test for cooling cycle, (c) tensile test

3.6 Membrane performance

3.6.1 Effect of beaded layer thickness

Membrane performance for electrospun membranes was examined before and after the electrospun surface morphology was altered through a surface modification via using different spray amount (1– 5 ml) of bead structure. Fig. 8 and Fig S2 shows the variation of flux and rejection over the course of five hours for the commercial, neat and modified membranes. The feed solution, with total concentration 2500 ppm of mix heavy metal element (Pb, Zn, Cd, Cu, Ni), was used as a simulated inorganically polluted wastewater. Additionally, the AGMD was operated at 60 ^{o}C and 7^{o}C as feed and coolant temperature, respectively, with a feed flow rate of 1.5 l/min. As can be seen from Fig. 8 the commercial membrane (HVHP) showed the lowest permeate flux, as expected, around 14.7 LMH. The neat membrane (ES15) showed a flux of the range between 20 to 19.5 LMH, while the control membrane with beads surface structure, but without NPs, (ES15-C) exhibited a flux of 20.5 LMH. The higher flux of both neat and control electrospun membranes compared with commercial membrane can be attributed to the electrospun membranes high porosity and surface hydrophobicity.

The flux trend of beaded structure membranes with varying spraying volume with alumina NPs in the polymer solution showed an interesting result. For instance, the flux increased for ES15-2 with the spinning volume to 2 ml by 12.5 % compare with the neat electrospun membrane (ES15). This might be due to enhanced membrane superhydrophobicity and

membrane surface roughness, which increased the surface evaporation area despite the reduction of the membrane porosity by 2.89%. In fact, the monolayer was created on modified membrane (ES15-2) minimized the pore wetting and delivered increased interface surface area to enhance mass transfer. Additionally, heat and mass transfer might improve in the membrane feed side sub-layer due to a decrease of the sub-layer thickness and increase in the Reynolds number as it explained by Zahirifar et al. [46]. However, an increase in the spray layer, as in membrane ES15-3 and ES15-5, lead to a slight reduction in membrane flux compared with ES15-2 which can be attributed to a reduction of membrane porosity and hydrophobicity. Accordingly, the permeate flux of ES15-3 and ES15-5 reduced by 3.5 % and 15.1%, respectively, compared with ES15-2 which is ascribed to sharp reduction of membrane porosity by 2.6% and 8.8%, and WCA by 1.3% and 2.3% respectively. Conversely, the permeate flux increases slightly from ES15-1 to ES15-2, which is likely due to the increased membrane hydrophobicity, despite a small decrease in porosity. As a result, the best conditions for permeate flux are found with membrane ES15-2, which had the best combination of high hydrophobicity and high porosity.

Control membrane (ES15-C) had lower flux than ES15-2, which has the same spray volume (2ml) used to generate the bead structure. This might be due to membrane surface hydrophobicity, in the case of ES15-C, leading to trapping of the feed solution in the beaded structure, reducing the evaporation area.

Aside from permeate flux, Fig. S2 and S3 illustrate the rejection percentage of each heavy metal element over time. Neat membrane (ES15) showed the lowest rejection percentage, in which the rejection percentage was between 90 and 82% for all heavy metals followed by ES15-C as shown in Fig. S3a with the rejection rate 99.2%. In comparison, commercial and modified membrane with NPs embedded in the bead structure as shown in Fig. S2 exhibited high rejection over 99.95%, with ES15-2 exhibiting the highest rejection rate above 99.99%.

3.6.2 Membrane stability

The beaded structure of the best performing modified membrane, ES15-2, was investigated in terms of stability by conducting SEM measurements before and after a 10 minutes sonication. Fig. 9 depicts the SEM and sonication test for tested membrane with 30 h in AGMD after flushed with deionized water. According to Fig. 9 the surface morphology of ES15-2 did not change. This suggests a high adhesion of beads to the membrane surface, which might be due to present the small diameter fibres which created a network between the beads and also to residual solvent left after electrospraying helping to increase the adhesion with the surface. The heat-press treatment at 160^{o}C, which is below the PVDF melting point (165^{o}C), would have played another role to further strengthen the bonding of the beads with the nanofibres.

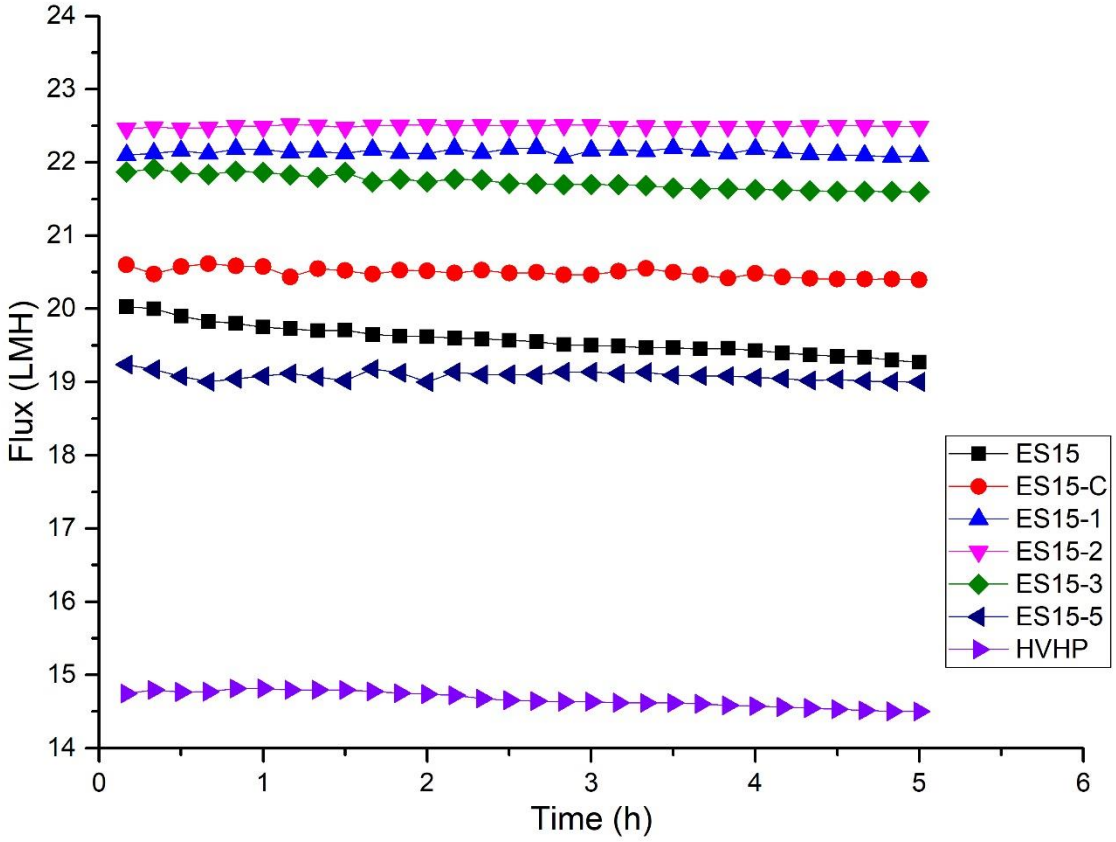

Fig. 8 Water permeability for commercial, neat and modified membrane during 5 hours.

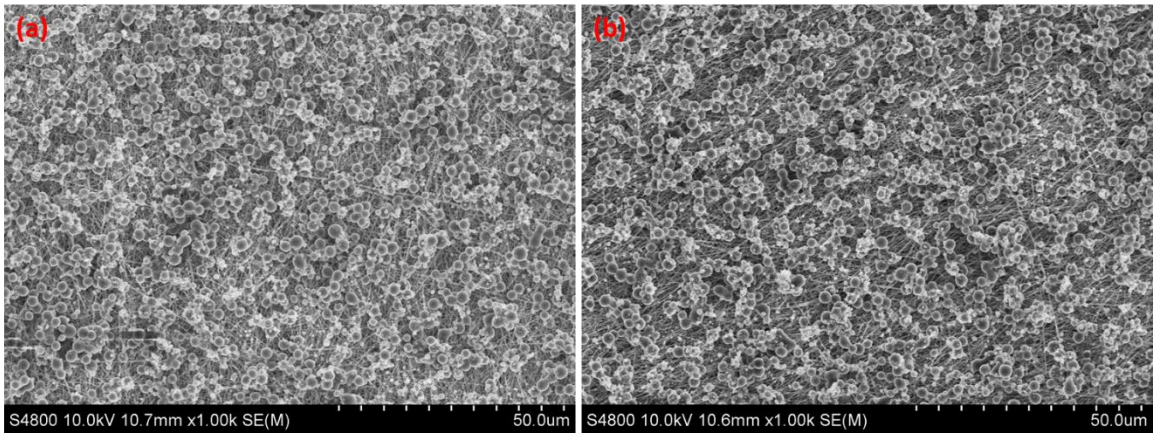

Fig. 9 SEM images of ES15-2 after 30h of operation (a) before sonication test, (b) after the sonication test.

3.6.3 Long term membrane stability

Membrane performance for long-time operation stability is one crucial factor to assess the suitability of a new membrane for MD application. Generally, both membrane wettability and permeate flux is consider the main goal for majority of the researchers to improve membrane fabrication technique. To make a fair comparison with other research, we conducted a long-term operation by using 60^{o}C as feed temperature while 20^{o}C as coolant temperature for the AGMD as an operating condition. Additionally, the feed solution was prepared by dissolving 600 ppm of each heavy metal element with final concentration 3.5 wt%. The MD test was carried out for 30 hours and the membrane performance were compare depends on permeate flux and conductivity. The modified electrospun membrane with highest performance (ES15-2) was selected for long-time tests alongside the commercial membrane HVHP. Fig. 10 shows both the change of the permeate flux and permeate conductivity with time of the tested membranes. It can be seen from Fig. 10a that the ES15-2 membrane has higher flux (18.6 LMH) compared with commercial membrane (12.5 LMH). The higher flux for ES15-2 was explained before due to its high hydrophobicity.

The electrical conductivity of the permeate shows an interesting result. It can be seen from Fig. 10b that the ES15-2 membrane maintained a very low permeate conductivity of less than 5 µs/cm. The results also reveal that the ES15-2 has stable permeate conductivity during 30-hour operation. This can be attributed to the high hydrophobicity of the surface which maintain during the operation. Additionally, the performance of optimum membrane (ES15-2) was compared with other AGMD membranes reported in the literature (Table 3). It can be seen that ES15-2 demonstrated better or suitable performance in terms of permeate flux and rejection. According to the results, the ES15-2 is a good candidate for AGMD applications, with an uncomplicated fabrication technique was used via electrospinning and electrospray methods.

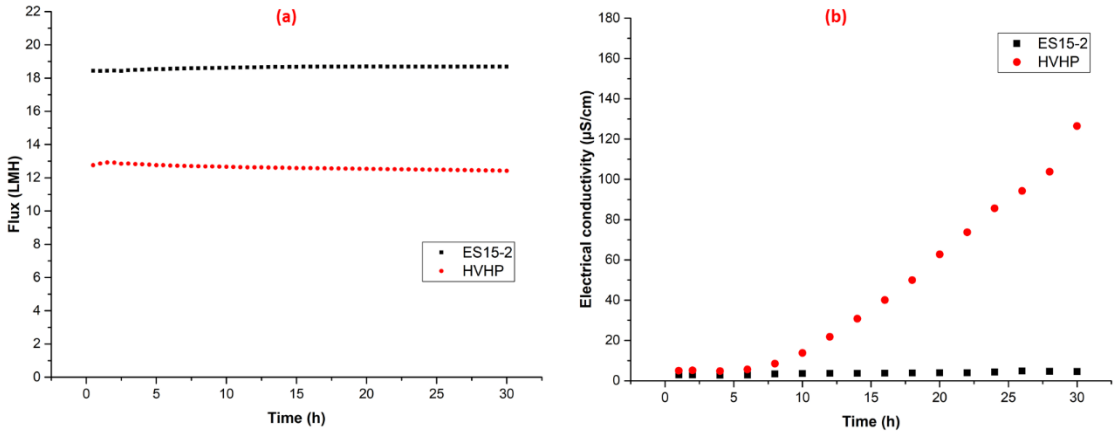

Fig. 10 Long-term operation run for ES15-2 and commercial membrane (a) permeate flux, (b) permeate conductivity.

Table 3. Comparison between Membrane properties of different PVDF membranes with surface modification and MD parameters in AGMD.

Membrane	Fabrication technique	Modification method	Membrane properties					AGMD parameters						Flux (LMH)	Rejection (%)	Ref
			Mean pore size (µm)	Porosity (%)	Thickness (µm)	WCA (°)	LEP (bar)	Feed temp (°C)	Feed flow rate (l/min)	Coolant temp. (°C)	Feed conc. (wt%)	Air gap (mm)	Testing time (h)			
PVDF/functionalized Graphene oxide (FGO)	Phase inversion	cast coating (PVDF+FGO)	0.057	60.5	85±1.2	146±1.1	1.85±0.12	80	15	15	3.5	1	120	16.7		[46]
PVDF/ functionalized silica aerogel	Phase inversion	layer-by-layer (silica aerogel)	0.09 ±0.01	79.4±1.6	62.4 ±1.0	>170	2.82±0.17	60	24	20	RO brine	3	24	10.55 - 11.93	100	[21]
ES15-2	Electrospinning	Electrospray (PVDF+Al_2O_3)	0.394	87.5 ±0.3	115±0.82	154	1..72	60	1.5	20	3.5	8.5	30	18.6	99.99	This study

4. Conclusion

In this study, a combination of electrospinning / electrospraying was used as a one-step fabrication technique to fabricate a superhydrophobic membrane with hierarchical micro- and nano-structured surface. The fabrication was achieved by spraying a micro-bead structure comprised of PVDF beads with combined with non-fluorinated superhydrophobic Al_2O_3 NPs on a PVDF electrospun membrane. A series of membrane characterizations were conducted on membrane surface and structure together with short and long-term operation by using mix solution of synthetic wastewater from heavy metals in AGMD application. The beads showed good stability on membrane surface using sonication tests. Varying the spraying time to adjust the bead layer structure lead to a that slight reduction in membrane pore size and a large reduction in membrane porosity with increase of the spraying volume while both LEP and WCA were boosted significantly. Modified membranes fabricated with 2 ml spray solution volume and 30 wt% Al_2O_3 NPs created a beaded surface structure with porosity (87.5%), mean pore size (0.39 µm), LEP (25 psi) and WCA (154°) adequate for AGMD applications. While the mechanical tests showed a noticeable reduction in elongation at break with increase of bead layer thickness. Thermal properties revealed an insignificant effect of bead structure on membrane melting point and crystallization structure. Additionally, ES15-2 membrane showed a high flux of 23 LMH and 99.99 % by using feed temperature and coolant of 60 °C and 7°C respectively. Long-term operation of the best performing membrane, with coolant temperature of 20°C and 3.5 wt% feed concentration, showed excellent performance in terms of flux at 18.6 LMH and 99.99% rejection. Results from this study indicate potential applications of PVDF-beaded structure surface in the treatment of water contaminated with inorganic compounds.

Acknowledgment

We gratefully acknowledge the finance support for the scholarship provide by the Ministry of Higher Education and Scientific Research/Iraq and Al-Mustansiriya University/Baghdad for the Ph.D. student (Hadi Attia). Also, we would like to thank Dr. Feras Korkees and Dr. Shirin Alexander for their help and support in performing membrane tensile testing and nanoparticle functionalization.

References

[1] L.D. Tijing, Y.C. Woo, J.-S. Choi, S. Lee, S.-H. Kim, H.K. Shon, Fouling and its control in membrane distillation—A review, Journal of Membrane Science, 475 (2015) 215-244.

[2] P. Wang, T.-S. Chung, Recent advances in membrane distillation processes: Membrane development, configuration design and application exploring, Journal of Membrane Science, 474 (2015) 39-56.

[3] O. Makanjuola, I. Janajreh, R. Hashaikeh, Novel technique for fabrication of electrospun membranes with high hydrophobicity retention, Desalination, 436 (2018) 98-106.

[4] B.S. Lalia, E. Guillen-Burrieza, H.A. Arafat, R. Hashaikeh, Fabrication and characterization of polyvinylidenefluoride-co-hexafluoropropylene (PVDF-HFP) electrospun membranes for direct contact membrane distillation, Journal of Membrane Science, 428 (2013) 104-115.

[5] A. Alkhudhiri, N. Darwish, N. Hilal, Membrane distillation: a comprehensive review, Desalination, 287 (2012) 2-18.

[6] A. Alkhudhiri, N. Darwish, N. Hilal, Treatment of high salinity solutions: Application of air gap membrane distillation, Desalination, 287 (2012) 55-60.

[7] M. Khayet, C. Cojocaru, Air gap membrane distillation: Desalination, modeling and optimization, Desalination, 287 (2012) 138-145.

[8] L.M. Camacho, L. Dumée, J. Zhang, J.-d. Li, M. Duke, J. Gomez, S. Gray, Advances in membrane distillation for water desalination and purification applications, Water, 5 (2013) 94-196.

[9] M. Rezaei, D.M. Warsinger, J.H. Lienhard V, M.C. Duke, T. Matsuura, W.M. Samhaber, Wetting phenomena in membrane distillation: Mechanisms, reversal, and prevention, Water Research, 139 (2018) 329-352.

[10] E. Celia, T. Darmanin, E.T. De Givenchy, S. Amigoni, F. Guittard, Recent advances in designing superhydrophobic surfaces, J Colloid Interf Sci, 402 (2013) 1-18.

[11] M.K. Sarkar, K. Bal, F. He, J. Fan, Design of an outstanding super-hydrophobic surface by electro-spinning, Appl Surf Sci, 257 (2011) 7003-7009.

[12] Y.C. Woo, L.D. Tijing, W.-G. Shim, J.-S. Choi, S.-H. Kim, T. He, E. Drioli, H.K. Shon, Water desalination using graphene-enhanced electrospun nanofiber membrane via air gap membrane distillation, Journal of Membrane Science, 520 (2016) 99-110.

[13] Z.-Q. Dong, X.-H. Ma, Z.-L. Xu, Z.-Y. Gu, Superhydrophobic modification of PVDF–SiO2electrospun nanofiber membranes for vacuum membrane distillation, RSC Adv., 5 (2015) 67962-67970.

[14] E.-J. Lee, A.K. An, T. He, Y.C. Woo, H.K. Shon, Electrospun nanofiber membranes incorporating fluorosilane-coated TiO 2 nanocomposite for direct contact membrane distillation, Journal of Membrane Science, 520 (2016) 145-154.

[15] M.R. Fouladi-Vanda1b, J. Karimi-Sabet, M.-A. Mousavian1a, Formation and characterization of a high hydrophobic membrane with functionalized GO by electrospinning for Air Gap Membrane Distillation.

[16] H. Attia, S. Alexander, C.J. Wright, N. Hilal, Superhydrophobic electrospun membrane for heavy metals removal by air gap membrane distillation (AGMD), Desalination, 420 (2017) 318-329.

[17] J. Prince, G. Singh, D. Rana, T. Matsuura, V. Anbharasi, T. Shanmugasundaram, Preparation and characterization of highly hydrophobic poly (vinylidene fluoride)–Clay nanocomposite nanofiber membranes (PVDF–clay NNMs) for desalination using direct contact membrane distillation, Journal of Membrane Science, 397 (2012) 80-86.

[18] S.S. Ray, S.-S. Chen, C.T.N. Dan, H.-T. Hsu, H.-M. Chang, N.C. Nguyen, H.-T. Nguyen, Casting of a superhydrophobic membrane composed of polysulfone/Cera flava for improved desalination using a membrane distillation process, Rsc Adv, 8 (2018) 1808-1819.

[19] S. Mallakpour, E. Khadem, Recent development in the synthesis of polymer nanocomposites based on nano-alumina, Progress in Polymer Science, 51 (2015) 74-93.

[20] Z. Zhu, Y. Liu, H. Hou, W. Shi, F. Qu, F. Cui, W. Wang, Dual-Bioinspired Design for Constructing Membranes with Superhydrophobicity for Direct Contact Membrane Distillation, Environmental science & technology, (2018).

[21] Y.C. Woo, Y. Kim, M. Yao, L.D. Tijing, J. Choi, S. Lee, S. Kim, H. Shon, Hierarchical Composite Membranes with Robust Omniphobic Surface Using Layer-By-Layer Assembly Technique, Environmental science & technology, (2018).

[22] F. Guo, A. Servi, A. Liu, K.K. Gleason, G.C. Rutledge, Desalination by membrane distillation using electrospun polyamide fiber membranes with surface fluorination by chemical vapor deposition, Acs Appl Mater Inter, 7 (2015) 8225-8232.

[23] S.M.S. Shahabadi, H. Rabiee, S.M. Seyedi, A. Mokhtare, J.A. Brant, Superhydrophobic dual layer functionalized titanium dioxide/polyvinylidene fluoride-co-hexafluoropropylene (TiO 2/PH) nanofibrous membrane for high flux membrane distillation, Journal of Membrane Science, 537 (2017) 140-150.

[24] J. Zhang, Z. Song, B. Li, Q. Wang, S. Wang, Fabrication and characterization of superhydrophobic poly (vinylidene fluoride) membrane for direct contact membrane distillation, Desalination, 324 (2013) 1-9.

[25] H. Attia, S. Alexander, C.J. Wright, N. Hilal, Superhydrophobic electrospun membrane for heavy metals removal by air gap membrane distillation (AGMD), Desalination, (2017).

[26] S. Alexander, J. Eastoe, A.M. Lord, F.d.r. Guittard, A.R. Barron, Branched hydrocarbon low surface energy materials for superhydrophobic nanoparticle derived surfaces, Acs Applied Materials & Interfaces, 8 (2015) 660-666.

[27] H. Attia, D.J. Johnson, C.J. Wright, N. Hilal, Comparison between dual-layer (superhydrophobic–hydrophobic) and single superhydrophobic layer electrospun membranes for heavy metal recovery by air-gap membrane distillation, Desalination, 439 (2018) 31-45.

[28] H. Attia, M.S. Osman, D.J. Johnson, C. Wright, N. Hilal, Modelling of air gap membrane distillation and its application in heavy metals removal, Desalination, 424 (2017) 27-36.

[29] B. Tarus, N. Fadel, A. Al-Oufy, M. El-Messiry, Effect of polymer concentration on the morphology and mechanical characteristics of electrospun cellulose acetate and poly (vinyl chloride) nanofiber mats, Alexandria Engineering Journal, 55 (2016) 2975-2984.

[30] G. Mago, D.M. Kalyon, F.T. Fisher, Membranes of polyvinylidene fluoride and PVDF nanocomposites with carbon nanotubes via immersion precipitation, Journal of Nanomaterials, 2008 (2008) 17.

[31] Y.J. Park, Y.S. Kang, C. Park, Micropatterning of semicrystalline poly (vinylidene fluoride)(PVDF) solutions, Eur Polym J, 41 (2005) 1002-1012.

[32] E.-J. Lee, B.J. Deka, J. Guo, Y.C. Woo, H.K. Shon, A.K. An, Engineering the re-entrant hierarchy and surface energy of PDMS-PVDF membrane for membrane distillation using a facile and benign microsphere coating, Environmental Science & Technology, 51 (2017) 10117-10126.

[33] N. Bock, M.A. Woodruff, D.W. Hutmacher, T.R. Dargaville, Electrospraying, a reproducible method for production of polymeric microspheres for biomedical applications, Polymers-Basel, 3 (2011) 131-149.

[34] Y. Liu, J.H. He, J.y. Yu, H.m. Zeng, Controlling numbers and sizes of beads in electrospun nanofibers, Polymer International, 57 (2008) 632-636.

[35] J. Wu, Y. Ding, J. Wang, T. Li, H. Lin, J. Wang, F. Liu, Facile fabrication of nanofiber- and micro/nanosphere-coordinated PVDF membrane with ultrahigh permeability of viscous water-in-oil emulsions, Journal of Materials Chemistry A, 6 (2018) 7014-7020.

[36] A. Deshmukh, C. Boo, V. Karanikola, S. Lin, A.P. Straub, T. Tong, D.M. Warsinger, M. Elimelech, Membrane distillation at the water-energy nexus: limits, opportunities, and challenges, Energy & Environmental Science, 11 (2018) 1177-1196.

[37] E. Drioli, A. Ali, F. Macedonio, Membrane distillation: Recent developments and perspectives, Desalination, 356 (2015) 56-84.

[38] A. Bahgat Radwan, A.M. Abdullah, A. Mohamed, M.A. Al-Maadeed, New Electrospun Polystyrene/Al2O3 Nanocomposite Superhydrophobic Coatings; Synthesis, Characterization, and Application, Coatings, 8 (2018) 65.

[39] Y. Liao, R. Wang, A.G. Fane, Fabrication of bioinspired composite nanofiber membranes with robust superhydrophobicity for direct contact membrane distillation, Environmental science & technology, 48 (2014) 6335-6341.

[40] I. Sas, R.E. Gorga, J.A. Joines, K.A. Thoney, Literature review on superhydrophobic self-cleaning surfaces produced by electrospinning, Journal of Polymer Science Part B: Polymer Physics, 50 (2012) 824-845.

[41] L. Feng, Y. Zhang, J. Xi, Y. Zhu, N. Wang, F. Xia, L. Jiang, Petal effect: a superhydrophobic state with high adhesive force, Langmuir, 24 (2008) 4114-4119.

[42] L.D. Tijing, Y.C. Woo, W.-G. Shim, T. He, J.-S. Choi, S.-H. Kim, H.K. Shon, Superhydrophobic nanofiber membrane containing carbon nanotubes for high-performance direct contact membrane distillation, Journal of Membrane Science, 502 (2016) 158-170.

[43] L.D. Tijing, J.-S. Choi, S. Lee, S.-H. Kim, H.K. Shon, Recent progress of membrane distillation using electrospun nanofibrous membrane, Journal of Membrane Science, 453 (2014) 435-462.

[44] P. Yazgan-Birgi, M.I. Hassan Ali, H.A. Arafat, Estimation of liquid entry pressure in hydrophobic membranes using CFD tools, Journal of Membrane Science, 552 (2018) 68-76.

[45] C. Kriegel, A. Arrechi, K. Kit, D. McClements, J. Weiss, Fabrication, functionalization, and application of electrospun biopolymer nanofibers, Critical reviews in food science and nutrition, 48 (2008) 775-797.

[46] J. Zahirifar, J. Karimi-Sabet, S.M.A. Moosavian, A. Hadi, P. Khadiv-Parsi, Fabrication of a novel octadecylamine functionalized graphene oxide/PVDF dual-layer flat sheet membrane for desalination via air gap membrane distillation, Desalination, 428 (2018) 227-239.